A Versatile Wavelet Domain Noise Filtration Technique for Medical Imaging

Aleksandra Pižurica, Wilfried Philips, Ignace Lemahieu, and Marc Acheroy

***Abstract*—In this paper, we propose a robust wavelet domain method for noise filtering in medical images. The proposed method adapts itself to various types of image noise as well as to the preference of the medical expert: a single parameter can be used to balance the preservation of (expert-dependent) relevant details against the degree of noise reduction.**

The algorithm exploits generally valid knowledge about the correlation of significant image features across the resolution scales to perform a preliminary coefficient classification. This preliminary coefficient classification is used to empirically estimate the statistical distributions of the coefficients that represent useful image features on the one hand and mainly noise on the other. The adaptation to the spatial context in the image is achieved by using a wavelet domain indicator of the local spatial activity. The proposed method is of low-complexity, both in its implementation and execution time. The results demonstrate its usefulness for noise suppression in medical ultrasound and magnetic resonance imaging. In these applications, the proposed method clearly outperforms single-resolution spatially adaptive algorithms, in terms of quantitative performance measures as well as in terms of visual quality of the images.

***Index Terms*—Noise reduction, wavelets, joint detection and estimation, generalized likelihood ratio.**

I. Introduction

In medical images, noise suppression is a particularly delicate and difficult task. A trade off between noise reduction and the preservation of actual image features has to be made in a way that enhances the diagnostically relevant image content. Image processing specialists usually lack the biomedical expertise to judge the diagnostic relevance of the denoising results. For example, in ultrasound images, speckle noise may contain information useful to medical experts [39]; the use of speckled texture for a diagnosis was discussed in [18], [35]. Also, biomedical images show extreme variability and it is necessary to operate on a case by case basis [36]. This motivates the construction of robust and versatile denoising methods that are applicable to various circumstances, rather than being optimal under very specific conditions. The notion of robustness in multiscale denoising was addressed in [19]. In this paper, we propose one robust method that adapts itself to various types of image noise as well as to the preference of the medical expert: a single parameter can be used to balance the preservation of (expert-dependent) relevant details against the degree of noise reduction.

In image denoising one often faces uncertainty about the presence of a given "feature of interest" (e.g., an image edge) in a noisy observation. Due to the sparsity of the wavelet representation, the Middleton's optimum coupled detection and estimation approach [28] seems well suited for wavelet domain image denoising. To the authors' knowledge such approaches have received little attention so far in wavelet domain filtering. Bayesian methods [2], [5], [37] take the uncertainty of the signal presence into account implicitly, assuming a Bernoulli process on the wavelet coefficients [20] and using Gaussian mixture models for the probability density functions of the wavelet coefficients. Related hereto, but more sophisticated, spatially adaptive methods usually employ complex algorithms, based on hidden Markov tree models [6], [10] or Markov random field prior models [17], [23], [31]. Other recent trends in wavelet-based image denoising include applying different types of filtering in supposedly smooth and supposedly heterogeneous or "edged" image regions [12], [21], spatially adaptive thresholding [4] and locally adaptive Wiener filtering [29].

Recently, we proposed an alternative, low-complexity joint detection and estimation method [32]. In particular, the method applies the minimum mean squared error criterion assuming that each wavelet coefficient represents a "signal of interest" with a probability $p < 1$, leading to the generalized likelihood ratio [28] formulation in the wavelet domain. In [32], we introduced an analytical model for the probability of signal presence, which is adapted to the global coefficient histogram and to a *local indicator of spatial activity* (e.g., the locally averaged magnitude of the wavelet coefficients).

In this paper, we propose a related, but more flexible method, which is applicable to various and unknown types of image noise. In particular, we do not rely on the exact prior knowledge of the noise distribution, which allows one to estimate the probability density function (pdf) of noise-free wavelet coefficients from the noisy histogram. Instead, we employ a preliminary detection of the wavelet coefficients that represent the features of interest in order to *empirically* estimate the conditional pdf's of the coefficients given the useful features and given background noise. At the same time, the preliminary coefficient classification is also exploited to empirically estimate the correspond-

A. Pižurica and W. Philips are with the Department for Telecommunications and Information Processing (TELIN), Ghent University, Sint-Pietersnieuwstraat 41, B-9000 Gent, Belgium. E-mail: Aleksandra.Pizurica@telin.rug.ac.be, philips@telin.rug.ac.be, Tel: +32 9 264 34 12, Fax: +32 9 264 42 95

I. Lemahieu is with the Department for Electronics and Information Systems (ELIS/MEDISIP), Ghent University, Sint-Pietersnieuwstraat 41, B-9000 Gent, Belgium. E-mail: ignace.lemahieu@rug.ac.be, Fax: 32-9-264.35.94, Tel: 32-9-264.42.32

M. Acheroy is with the Royal Military Academy, Av. de la Renaissance 30, B-1000 Brussels, Belgium. E-mail: acheroy@elec.rma.ac.be, Fax: +32 2 737 64 72, Tel.: + 32 2 737 64 70

ing conditional pdf's of the local spatial activity indicator. The preliminary classification step in the proposed method relies on the persistence of useful wavelet coefficients across the scales [25], and is related to the one in [38], but avoids its iterative procedure. In contrast to [38], and related methods like [11], [15], where the inter-scale correlations between wavelet coefficients are used for a "hard" selection of the coefficients from which the denoised image is reconstructed, our algorithm performs a soft modification of the coefficients adapted to the spatial image context.

The classification step of the proposed method involves an adjustable parameter that is related to the notion of the expert-defined "relevant image features". In certain applications the optimal value of this parameter can be selected as the one that maximizes the signal-to-noise ratio (SNR) and the algorithm can operate as fully automatic. However, we believe that in most medical applications the tuning of this parameter leading to a gradual noise suppression may be advantageous. The proposed algorithm is simple to implement and fast. We demonstrate its usefulness for denoising and enhancement of the ultrasound and the magnetic resonance images.

The paper is organized as follows. In Section II, the theoretical concept behind the proposed method and the new, practical algorithm are described. The application of the proposed method to ultrasound images is demonstrated and discussed in Section III. In Section IV, noise removal from the magnetic resonance images is addressed. The method is discussed in Section V, and the concluding remarks are in Section VI.

II. Proposed Method

A. Notation and Model Assumptions

In a wavelet decomposition of an image [24] a wavelet coefficient $w_{k,j}^D$ represents its bandpass content at resolution scale 2^j $(1 \leq j \leq J)$, spatial position k and orientation D. The lowpass image content is represented by scaling coefficients $u_{k,J}$. Typically, three orientation subbands are used: $D \in \{LH, HL, HH\}$, leading to three *detail images* at each scale, characterized by horizontal, vertical and diagonal directions. We use a *non-decimated* wavelet transform, with an equal number of coefficients at each resolution scale. The algorithm is implemented using the quadratic spline wavelet [25], as in [23], [38]. Whenever there can be no confusion, we omit the indices of the wavelet coefficients that denote the scale and the orientation. We start from a general noise model $w_k = y_k \oplus n_k$, where y_k is the unknown noise-free wavelet coefficient, $\oplus$ a point-wise mathematical operation and n_k an arbitrary noise contribution. Our wavelet domain estimation approach relies on the joint detection and estimation theory [28] and is related to the problem of the spectral amplitude estimation in [1], [9], [26].

Let X_k denote a random variable, which takes values x_k from the binary label set $\{0, 1\}$. The hypothesis "the wavelet coefficient w_k represents a signal of interest" is equivalent to the event $X_k = 1$, and the opposite hypothesis is equivalent to $X_k = 0$. The wavelet coefficients representing the signal of interest in a given subband are identically distributed random variables with the probability density function $p_{W_k|X_k}(w_k|1)$. Similarly, the coefficients in the same subband, corresponding to the absence of the signal of interest, are random variables with the pdf $p_{W_k|X_k}(w_k|0)$.

Under our model assumptions, the minimum mean squared error estimate (the conditional mean) of y_k is $\hat{y}_k = E(y_k|w_k, X_k = 1)P(X_k = 1|w_k) + E(y_k|w_k, X_k = 0)P(X_k = 0|w_k)$, where $E(\cdot)$ stands for the expected value. We proceed with the simplifications equivalent to those in [1]. If the signal of interest is surely absent in a given wavelet coefficient, then $y_k \simeq 0$ and $E(y_k|w_k, X_k = 0) \simeq 0$. In the case where the signal of interest is surely present, we approximate $E(y_k|w_k, X_k = 1) \simeq w_k$ which accounts for the fact that vast majority of the coefficient magnitudes representing the signal of interest are highly above the noise level. Applying Bayes' rule, one can express $P(X_k = 1|w_k)$ as a generalized likelihood ratio [28], and our estimate becomes

$$\hat{y}_k = \frac{\xi_k \mu_k}{1 + \xi_k \mu_k} w_k, \tag{1}$$

where

$$\xi_k = \frac{p_{W_k|X_k}(w_k|1)}{p_{W_k|X_k}(w_k|0)}, \quad \mu_k = \frac{P(X_k = 1|\mathcal{P})}{P(X_k = 0|\mathcal{P})}, \tag{2}$$

and $\mathcal{P}$, like in [1], symbolically denotes the prior knowledge that is used to estimate the probability of signal presence. In [32], we proposed a method to estimate this probability for each wavelet coefficient from its local surrounding, using a chosen indicator e_k of the local spatial activity. In particular, since our estimate of the probability of signal presence is a function of e_k, we write $P(X_k = 1|\mathcal{P}) = P(X_k = 1|e_k)$, and replace μ_k in (2) by

$$\hat{\mu}_k = \frac{P(X_k = 1|e_k)}{P(X_k = 0|e_k)} = r \, \frac{p_{E_k|X_k}(e_k|1)}{p_{E_k|X_k}(e_k|0)}, \tag{3}$$

where r is the ratio of unconditional prior probabilities

$$r = \frac{P(X_k = 1)}{P(X_k = 0)}. \tag{4}$$

For a given type of noise, one can derive the complete estimator analytically [32]. In such approaches, where the required conditional densities need to be analytically expressed, the choice of the local spatial activity indicator is usually restricted to simple forms: even when e_k is defined simply as the locally averaged coefficient magnitude, certain simplifying assumptions about the statistical properties of the wavelet coefficients are needed in order to derive $p_{E_k|X_k}(e_k|x_k)$ analytically. The algorithm that we propose in this paper is applicable to various noise types, and allows an arbitrary choice of e_k.

B. The New Algorithm

The idea behind the proposed algorithm is to empirically estimate the probabilities and the probability density functions that specify the estimator (1). Let N denote

the number of wavelet coefficients in a detail image. For each detail image $\mathbf{w}_j^D = \{w_{1,j}^D ... w_{N,j}^D\}$, we first estimate the *mask* $\hat{\mathbf{x}}_j^D = \{\hat{x}_{1,j}^D ... \hat{x}_{N,j}^D\}$, which indicates the positions of significant wavelet coefficients (representing the signal of interest). As usual, we relate the notion of significant wavelet coefficients to the standard deviation of the noise [17], [25]. Also, we rely on the persistence of significant wavelet coefficients across resolution scales [25], [38]. In particular, we extend our robust coarse-to-fine classification method from [33] as follows:

$$\hat{x}_{k,j}^D = \begin{cases} 0, & \text{if} \quad |w_{k,j}^D||\hat{y}_{k,j+1}^D| < (K\hat{\sigma}_j^D)^2, \\ 1, & \text{if} \quad |w_{k,j}^D||\hat{y}_{k,j+1}^D| \geq (K\hat{\sigma}_j^D)^2, \end{cases} \tag{5}$$

where $\hat{\sigma}_j^D$ is an estimate of the noise standard deviation in the detail image $\mathbf{w}_j^D$, and K is a heuristic, tunable parameter that controls the notion of the signal of interest. We estimate the standard deviation of the input noise $\hat{\sigma}$ as the median absolute deviation of the wavelet coefficients in the HH subband at the finest resolution scale, divided by 0.6745 [7]. In estimating $\hat{\sigma}_j^D$, we follow [12]: $(\hat{\sigma}_j^D)^2 = S_j^D \hat{\sigma}^2$, where for each subband the constant S_j^D is calculated from the filter coefficients of the highpass filter $\mathbf{g}$ and the lowpass filter $\mathbf{h}$ of the discrete wavelet transform, as $S_j^{LH,HL} = \left(\sum_k g_k^2\right)\left(\sum_l h_l^2\right)^{2j-1}$, and $S_j^{HH} = \left(\sum_k g_k^2\right)^2\left(\sum_l h_l^2\right)^{2(j-1)}$. To initialize the classification (5), we start from $\hat{\mathbf{y}}_J^D = \mathbf{w}_J^D$, where J is the coarsest resolution level in the wavelet decomposition.

Now we address the estimation of the wavelet coefficients $\mathbf{w}_j^D$ using the estimated mask $\hat{\mathbf{x}}_j^D$. The estimator (1) requires the conditional densities $p_{W_k|X_k}(w_k|x_k)$ and $p_{E_k|X_k}(e_k|x_k)$. Since $p_{W_k|X_k}(w_k|x_k)$ is usually highly symmetrical around 0, in practice we shall rather estimate the conditional pdf's $p_{M_k|X_k}(m_k|x_k)$ of the coefficient *magnitudes* $m_k = |w_k|$. As the local spatial activity indicator e_k, we use the averaged energy of the neighboring coefficients of w_k, where the neighbors are the surrounding coefficients in a square window at the same scale and the "parent" (i.e., the coefficient at the same spatial position at the first coarser scale). Having the estimated mask $\hat{\mathbf{x}} = \{\hat{x}_1 ... \hat{x}_N\}$, let $S_0 = \{k : \hat{x}_k = 0\}$ and $S_1 = \{k : \hat{x}_k = 1\}$. The empirical estimates $\hat{p}_{M_k|X_k}(m_k|0)$ and $\hat{p}_{E_k|X_k}(e_k|0)$ are computed from the histograms of $\{m_k : k \in S_0\}$ and $\{e_k : k \in S_0\}$, respectively (by normalizing the area under the histogram). Similarly, $\hat{p}_{M_k|X_k}(w_k|1)$ and $\hat{p}_{E_k|X_k}(e_k|1)$ are computed from the corresponding histograms for $k \in S_1$.

Our estimation approach still requires the probability ratio (4). Reasoning that $P(X_k = 1)$ can be estimated as the fractional number of labels for which $\hat{x}_k = 1$, we estimate the parameter r from (4) as

$$\hat{r} = \frac{\sum_{k=1}^N \hat{x}_k}{N - \sum_{k=1}^N \hat{x}_k}. \tag{6}$$

The practical estimator that we apply is thus

$$\hat{y}_k = \frac{\hat{r}\hat{\xi}_k\hat{\eta}_k}{1 + \hat{r}\hat{\xi}_k\hat{\eta}_k} w_k, \tag{7}$$

where

$$\hat{\xi}_k = \frac{\hat{p}_{M_k|X_k}(m_k|1)}{\hat{p}_{M_k|X_k}(m_k|0)}, \quad \text{and} \quad \hat{\eta}_k = \frac{\hat{p}_{E_k|X_k}(e_k|1)}{\hat{p}_{E_k|X_k}(e_k|0)}. \tag{8}$$

In Fig. 1, we show an example of the empirical densities $\hat{p}_{M_k|X_k}(m_k|x_k)$ and $\hat{p}_{E_k|X_k}(e_k|x_k)$. The direct computation of the ratios $\hat{\xi}_k$ and $\hat{\eta}_k$ from the normalized histograms shown in Fig. 1 is not appropriate due to errors in the tails. One solution is to first fit a certain distribution to the histogram. Here we apply a simpler approach, observing that both $\log(\hat{\xi}_k)$ and $\log(\hat{\eta}_k)$ can be approximated well by fitting a piece-wise linear curve as illustrated in Fig. 1. Formally, we approximate

$$\log(\hat{\xi}_k) \simeq \begin{cases} a_1 + b_1 m_k, & \hat{\xi}_k < 1, \\ a_2 + b_2 m_k, & \hat{\xi}_k \geq 1, \end{cases} \tag{9}$$

$$\log(\hat{\eta}_k) \simeq \begin{cases} c_1 + d_1 e_k, & \hat{\eta}_k < 1, \\ c_2 + d_2 e_k, & \hat{\eta}_k \geq 1. \end{cases} \tag{10}$$

The fitting in (9) is done as follows. For the index set $R_\xi = \{l : \hat{p}_{M|X}(m_l|0) \neq 0, \hat{p}_{M|X}(m_l|1) \neq 0\}$, we compute the log-ratios $\xi_{\mathbf{log}} = \{\log(\hat{p}_{M|X}(m_l|1)) - \log(\hat{p}_{M|X}(m_l|0)) : l \in R_\xi\}$. Further on, let $R_{\xi,1} = \{l : l \in R_\xi, \xi_{log,l} < 0\}$ and $R_{\xi,2} = \{l : l \in R_\xi, \xi_{log,l} \geq 0\}$. We look for the polynomial coefficients a_1, b_1, which minimize $\sum_{l \in R_{\xi,1}} (a_1 m_l + b_1 - \xi_{log,l})^2$, and the polynomial coefficients a_2, b_2, which minimize $\sum_{l \in R_{\xi,2}} (a_2 m_l + b_2 - \xi_{log,l})^2$, i.e., which are optimal in the least-square sense. The equivalent procedure is applied to find the coefficients c_1, d_1 and c_2, d_2 in (10).

This completes the specification of the proposed method; the algorithm is summarized in the Appendix. We demonstrate next its applications, using $J = 4$ decomposition levels.

III. Application to Ultrasound Images

Ultrasound images are corrupted by speckle noise [13], [39], which affects all coherent imaging systems. Fig. 2 illustrates the examples of gradual speckle suppression using the proposed method. The results in this figure correspond to the window size 5x5 and different values of the tuning parameter K in (5). The results demonstrate that the increase of K leads to a stronger suppression of the background texture and to the enhancement of sharp intensity variations.

To investigate the quantitative performance of the method, we use images with artificial speckle noise. A speckled image $\mathbf{d} = \{d_1 ... d_N\}$ is commonly modelled as [3], [34] $d_k = f_k v_k$, where $\mathbf{f} = \{f_1 ... f_N\}$ is a reference noise-free image, and $\mathbf{v} = \{v_1 ... v_N\}$ is a unit mean random field. Realistic spatially correlated speckle noise v_k in ultrasound images can be simulated by lowpass filtering a complex Gaussian random field and taking the magnitude of the filtered output [34]. We perform the lowpass filtering by averaging the complex values in a 3x3 sliding window. Such a short-term correlation was found sufficient [3] to model the realistic images well. By changing the variance of the underlying complex Gaussian random

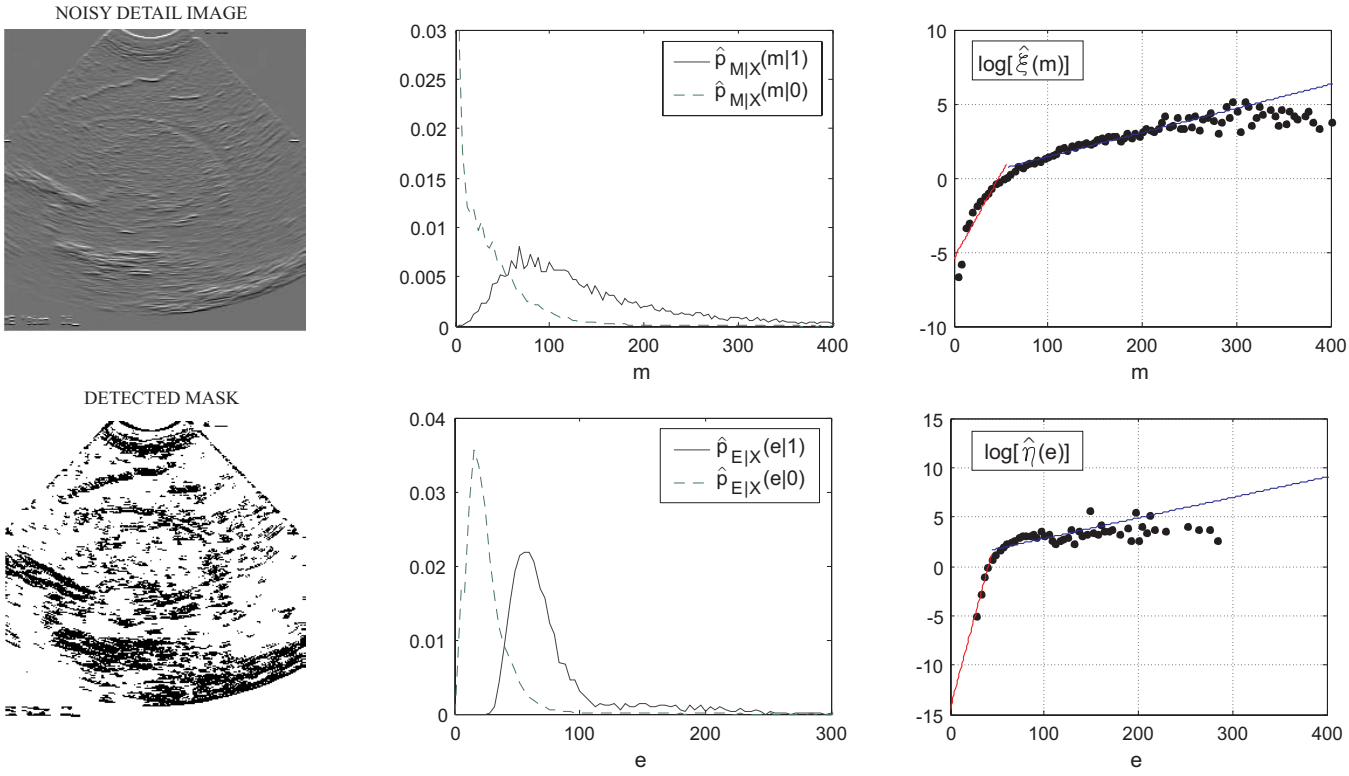

Fig. 1. Examples of the empirical pdf's and fitted log-ratios in the proposed method, for the top left ultrasound image from Fig. 2.

field, we generate images with different levels of speckle noise. We use two types of reference noise-free images: (1) realistic ultrasound images from Fig. 3, in which natural speckle noise was previously suppressed by the proposed method, and (2) a purely synthetic image in Fig. 4, which consists of regions with uniform intensity, sharp edges, and strong scatterers. As a quantitative performance measure, we use the signal to noise ratio in dB, defined as

$$SNR = 10\log(P_s/P_n), \tag{11}$$

where P_s is the variance of the noise-free reference image, and P_n is the noise variance. Regarding the noise suppression performance, the proposed method shows a stable behavior with respect to the tuning parameter K. Fig. 6 demonstrates that for different noise levels and for different test images the same value of this parameter ($K = 3$) can be chosen to provide a nearly maximum output SNR. It can also be seen that the window size 3x3 is optimal under the assumed speckle model.

We compare the performance of the proposed method to one conventional approach in speckle filtering: the homomorphic Wiener filter [3], [16]. In particular, we apply Matlab's spatially adaptive Wiener filter to the image logarithm and subsequently perform the exponential transformation on the filtered output. The window size of the Wiener filter was experimentally optimized to produce the maximum output SNR for each test image and for each amount of noise used in the simulations. The results clearly demonstrate that the proposed filter outperforms the homomorphic spatially adaptive Wiener filtering both in terms of SNR (Fig. 7) and in terms of the visual quality (Fig. 3 and Fig. 4). Finally, Fig. 5 enables us to make a visual comparison of the results of the proposed method and the homomorphic Wiener filter on a real image without synthetic noise.

IV. Application to MRI Images

In magnetic resonance imaging [8], [14], [22], [27] the practical limits of the acquisition time impose a trade-off between the signal to noise ratio and the image resolution. The MRI image is commonly reconstructed by computing the inverse discrete Fourier transform of the raw data. Most commonly, the magnitude of the reconstructed image is used for visual inspection and for computer analysis. Noise in the MRI image magnitude is Rician [30], having a signal dependent mean.

Previously proposed wavelet domain filtering techniques were based on different thresholding schemes [30], [40], including [38], where the coefficient selection was based on inter-scale correlations. Our algorithm offers an additional functionality, which is the adaptation to the local spatial context.

In [30], it was noted that, due to the signal-dependent mean of the Rician noise, both wavelet and scaling coefficients of a noisy MRI image are *biased* estimates of their noise-free counterparts. It was shown that one can efficiently overcome this problem by filtering the *square* of the MRI magnitude image in the wavelet domain. In the squared magnitude image, data are non-central chi-square distributed, and the wavelet coefficients are no longer bi-

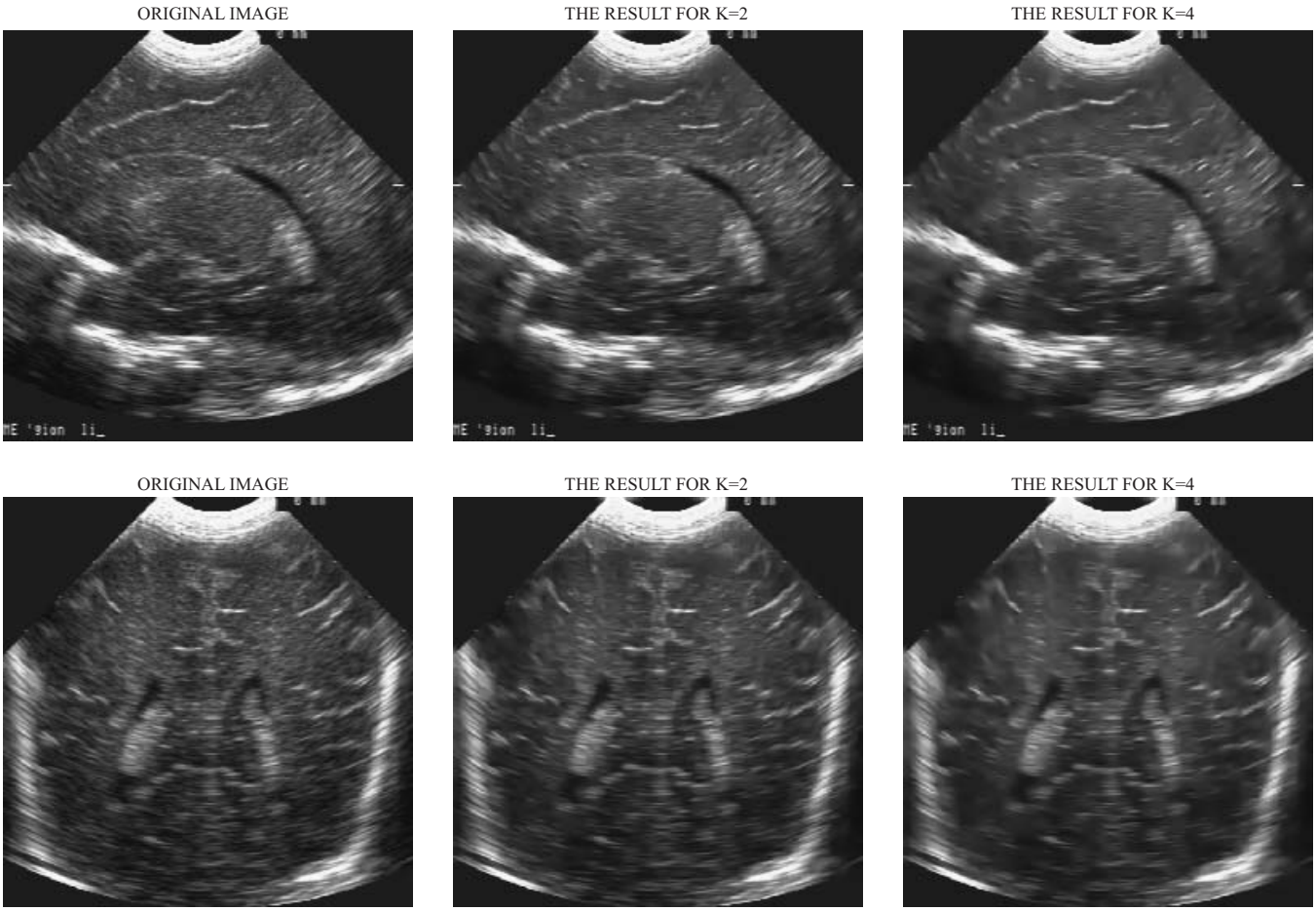

Fig. 2. Gradual noise suppression in ultrasound images using the proposed method.

ased estimates of their noise-free counterparts. The bias still remains in the scaling coefficients, but is not signal-dependent and it can be removed easily [30]: at the resolution scale 2^j, from each scaling coefficient $2^{j+1}\sigma_c$ should be subtracted, where σ_c^2 is the underlying complex Gaussian noise variance. We therefore apply our method to the squared magnitude of the MRI image, subtract the constant bias from the scaling coefficients, and subsequently compute the square root of the denoised squared-magnitude image.

First, we illustrate the performance of the proposed method on an MRI image with artificially added noise, and compare it to the spatially adaptive Wiener filter. The reference ("noise-free") image is a sufficiently clean, original MRI image of a human brain shown as the top left image in Fig. 8. In simulations, complex zero mean white Gaussian noise with standard deviation σ_c was added to this image. The top right image in Fig. 8 shows the noisy MRI magnitude for $\sigma_c = 30$. The denoising result of the proposed method, shown in Fig. 8 clearly outperforms the result of the spatially adaptive Wiener filtering.

The quantitative performance of the method, for the 3x3 window size is illustrated in Fig. 9. For different noise levels the optimal value of K is in the range [1.8, 2], and the algorithm shows a stable behavior with respect to K. In our experiments, on a number of different reference MRI images, the improvement over the spatially adaptive Wiener filtering was at least 0.5 dB (for relatively clean images) and more than 3 dB for low SNR images. In Fig. 9(b), we illustrate such a comparison between the two filters for the reference image from Fig. 8. For the Wiener filter, the window size was optimized for each noise level, to produce maximum output SNR.

The application of the proposed method to real noisy MRI images is demonstrated in Fig. 10. The MRI images were provided by the University hospital of Ghent. The noise suppression in these images is expected to facilitate further automatic processing, like e.g., segmentation.

V. Discussion

The proposed denoising method involves one adjustable parameter, K. For MRI images, its optimal value in terms of SNR is $K \approx 2$. For ultrasound images, we found the value $K = 3$ optimal under the assumed speckle model. In practice, a wide range of other values can be used; the adjustment is left to the medical expert who finally controls the image interpretation. Increasing the value of K leads to an increased smoothing of weak image textures while

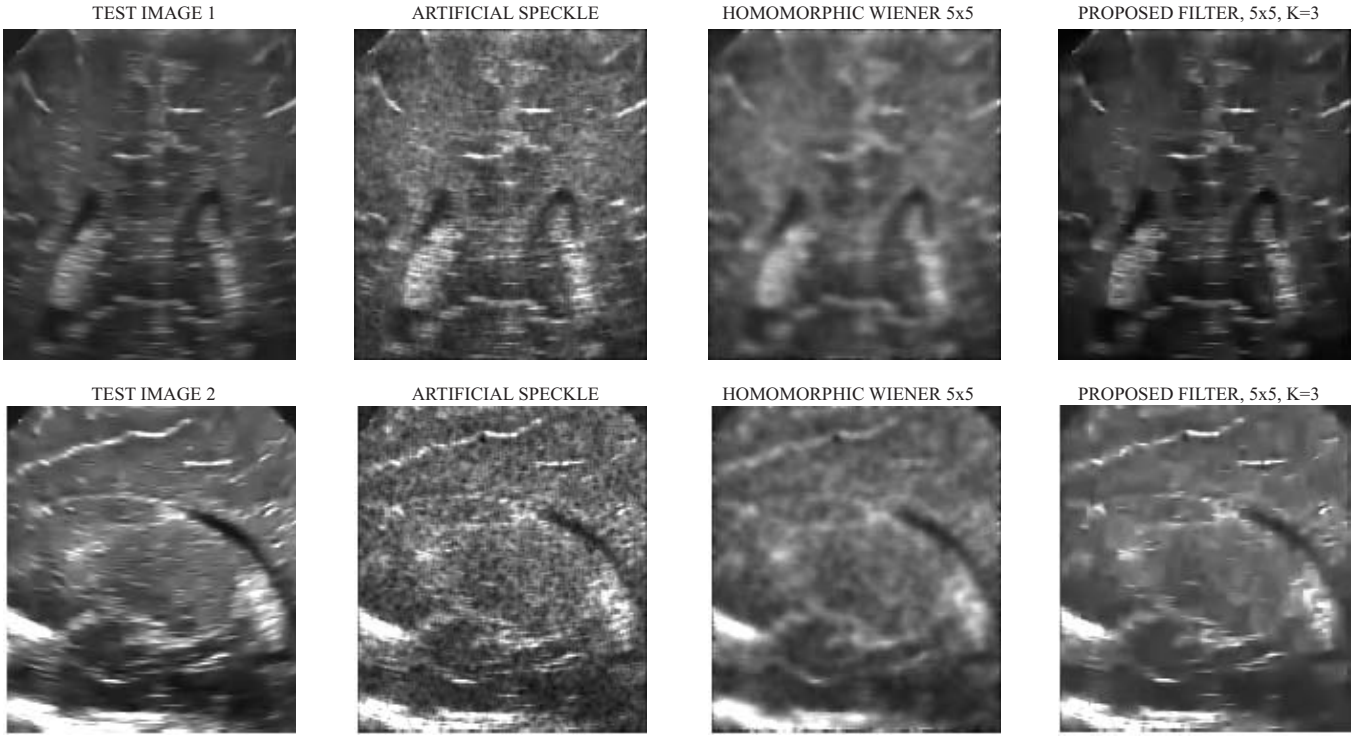

Fig. 3. From left to right: test images, artificially speckled images, the results of the homomorphic spatially adaptive Wiener filter, and the results of the proposed method, for $K = 3$ and window size 5x5.

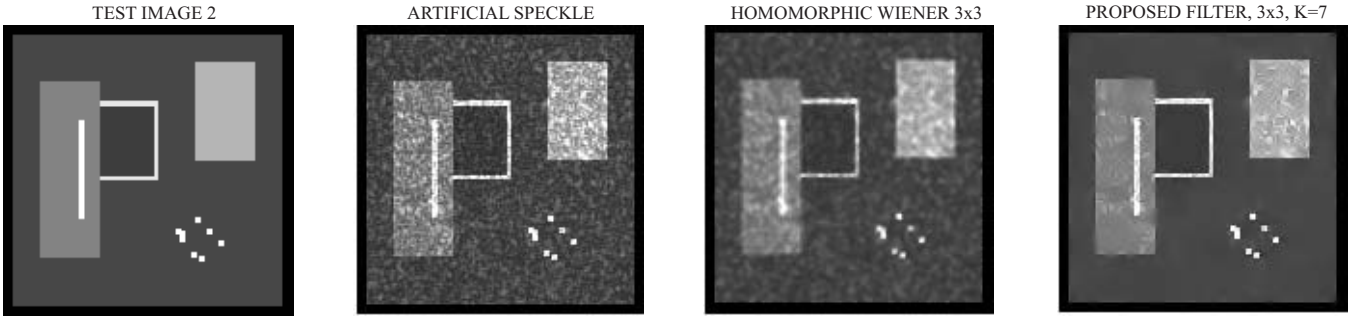

Fig. 4. From left to right: synthetic test image, artificially speckled image (SNR=8.7 dB), the result of the homomorphic spatially adaptive Wiener filter (SNR=11.3 dB), and the result of the proposed method (SNR=15.0 dB), for $K = 7$ and window size 3x3.

enhancing the presence of the main image discontinuities, as shown in Fig. 2.

The tuning of the parameter K may also be interpreted as (partly) compensating the errors introduced in estimating the noise standard deviation σ_J^D, which is required for the preliminary coefficient classification (5). In our algorithm, the estimates $\hat{\sigma}_j^D$ are found following [12] and are quite accurate for spatially non correlated noise. A more involved statistical modelling is required to estimate σ_j^D accurately for correlated speckle in ultrasound images. In our experiments, the use of accurate values of σ_j^D instead of the estimated ones did not improve the noise suppression performance of the proposed method significantly.

The local spatial activity indicator e_k in the proposed method is computed by locally averaging the neighboring coefficient magnitudes. The window size 3x3 was found optimal, in terms of SNR, both for ultrasound and for MRI images. It would be interesting to investigate the use of other forms for e_k. For example, the influence of the neighboring coefficients could be weighted according to their distance from the central coefficient and/or other than squared window shapes can be used.

We used four decomposition levels of the wavelet transform. Using more levels did not seem to improve the noise suppression performance.

VI. Conclusion

In this paper, we proposed a new, robust and efficient wavelet domain denoising technique, which is applicable to various types of image noise. The proposed method is in particular interesting for medical image denoising, since it accounts for the preference of the medical expert: a

Fig. 5. An original ultrasound image (left) and the results of the Homomorphic Wiener filter (middle) and the proposed filter (right). The window size for both filters is 3x3.

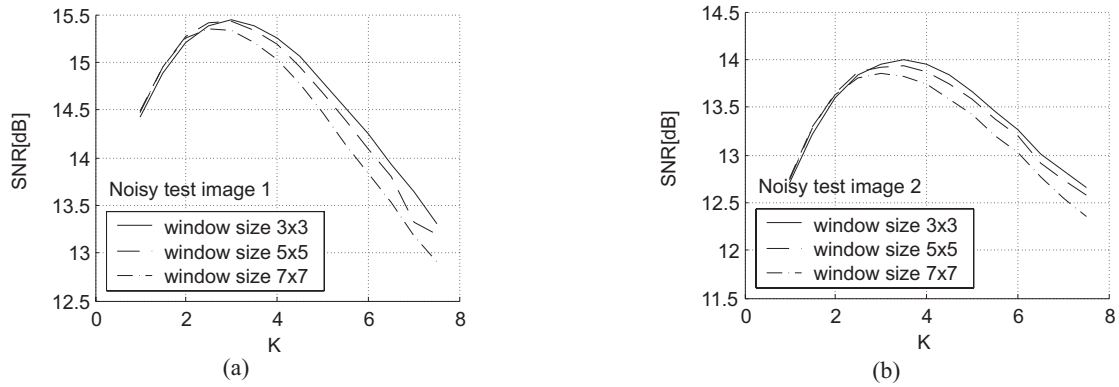

Fig. 6. The performance of the proposed method as a function of the value of the parameter K. (a) Test image 1 from Fig.3, input SNR=13.6 dB. (b) Test image 2 from Fig.3, input SNR=11.6 dB.

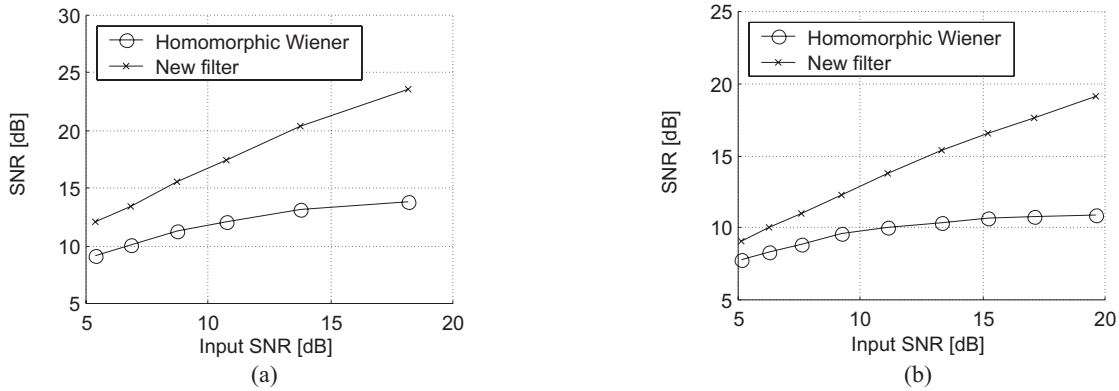

Fig. 7. Comparison between the proposed filter and the homomorphic Wiener filter. (a) The synthetic test image from Fig. 4. (b) The top left ultrasound image from Fig. 3.

single parameter can be used to balance the preservation of (expert-dependent) relevant details against the degree of noise reduction. Such a user interaction is in the first place useful for speckle noise removal from the ultrasound images. The proposed method is of low-complexity, both in its implementation and execution time. It adapts itself to unknown noise distributions and to the local spatial image context. We demonstrated its usefulness for noise suppression in ultrasound and in MRI images.

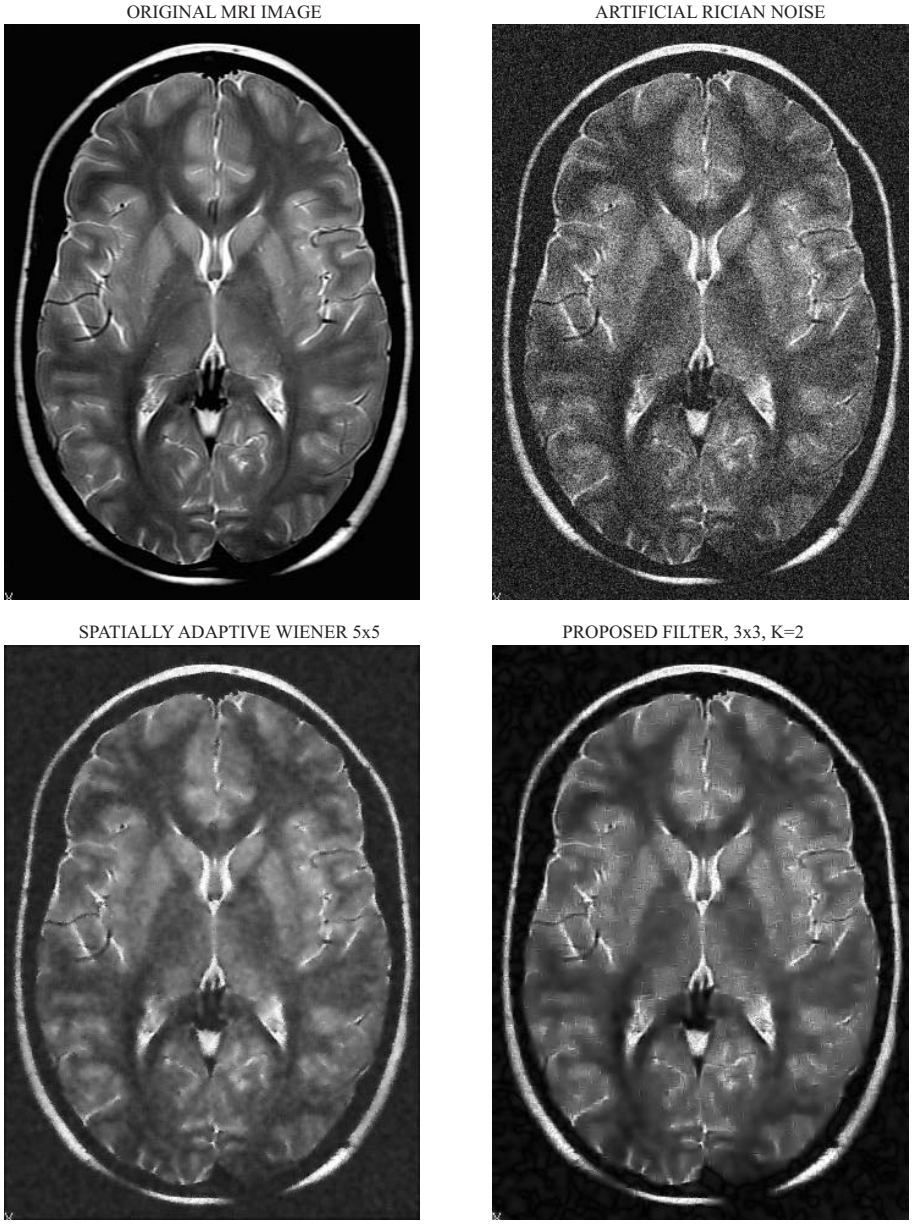

Fig. 8. Top left: original MRI image. Top right: image with artificial Rician noise ($\sigma_c = 30$, SNR=5.9 dB). Bottom left: the result of the spatially adaptive Wiener filtering (SNR=10.1 dB). Bottom right: the result of the proposed method for $K = 2$ and 3x3 window size (SNR=12.9 dB).

VII. Appendix

The algorithm described in Section II. B can be summarized briefly as follows:

- Compute the non decimated wavelet transform with J resolution levels.
- Initialize $\hat{\mathbf{y}}_J^D = \mathbf{w}_J^D$, $D \in \{HL, LH, HH\}$.
- For each orientation D and for each scale 2^j, $j = 1, ..., J-1$
  - For all the spatial positions $k = 1, ..., N$
    - Apply (5) yielding the label estimate $\hat{x}_k$.
    - Compute the local spatial activity indicator e_k.
  - Compute $\hat{r} = \sum_{l=1}^{N} \hat{x}_l / (N - \sum_{l=1}^{N} \hat{x}_l)$.
  - Define $S_0 = \{l : \hat{x}_l = 0\}$ and $S_1 = \{l : \hat{x}_l = 1\}$ and estimate $\hat{p}_{M|X}(m|0)$, $\hat{p}_{M|X}(m|1)$, $\hat{p}_{E|X}(e|0)$ and $\hat{p}_{E|X}(e|1)$, from the corresponding histograms of $m_l = |w_l|$ and e_l over $l \in S_0$ and over $l \in S_1$.
  - Fit the log-ratios $\log(\xi_k)$ and $\log(\eta_k)$ from (9) and (10).
  - For $k = 1, ..., N$: $\hat{y}_k = \hat{r}\hat{\xi}_k\hat{\eta}_k / (1 + \hat{r}\hat{\xi}_k\hat{\eta}_k) w_k$.
- Apply the inverse wavelet transform.

References

[1] T. Aach and D. Kunz, "Anisotropic spectral amplitude estimation for noise reduction and image enhancement," *Proc. IEEE Internat. Conf. on Image Proc., ICIP96*, pp. 335–338, Lausanne, Switzerland, 1996.

[2] F. Abramovich, T. Sapatinas, and B. W. Silverman, "Wavelet

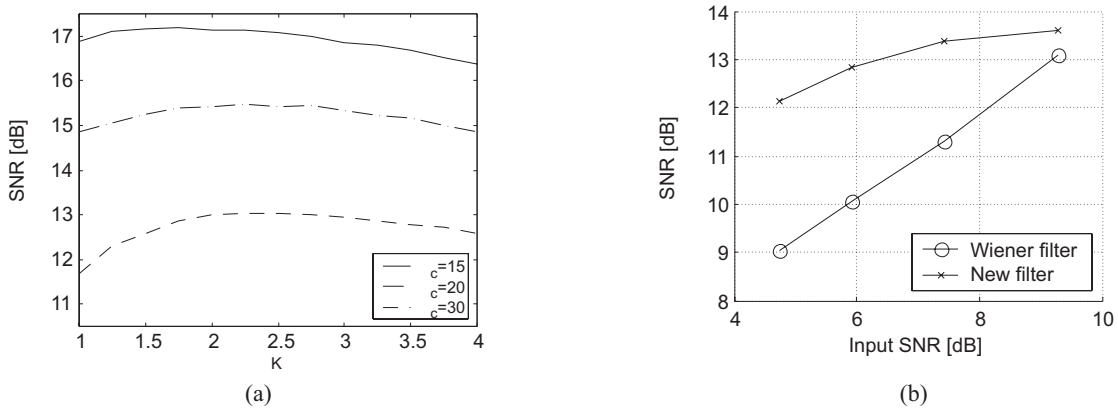

Fig. 9. Quantitative performance of the proposed method. (a) Influence of the parameter K for different values σ_c of the underlying complex Gaussian noise. (b) Noise suppression performance (for $K = 2$) in comparison to the spatially adaptive Wiener filtering. The original MRI image from Fig. 8 is used in the simulations.

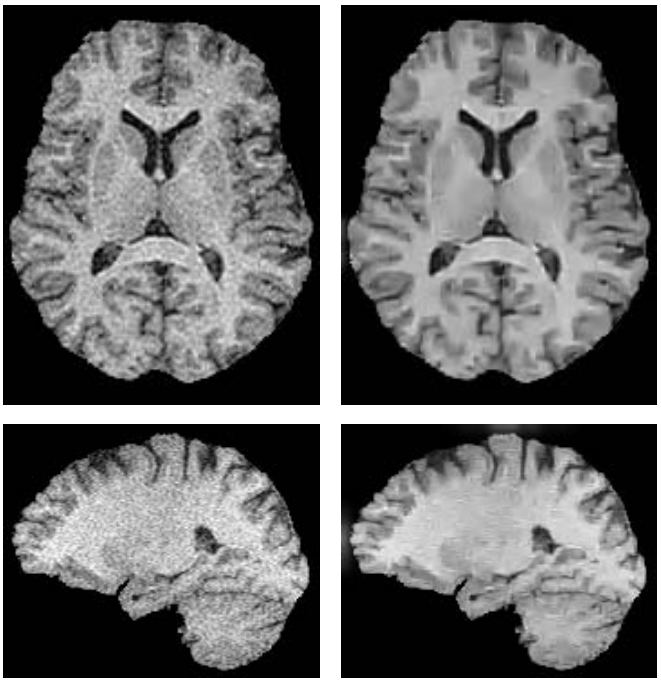

Fig. 10. Application to real noisy MRI images. Left: original images, right: the results of the proposed method for $K = 2$ and a 3x3 window size.

thresholding via a Bayesian approach," *J. of the Royal Statist. Society B*, vol. 60, pp. 725–749, 1998.

[3] A. Achim, A. Bezerianos, and P. Tsakalides, "Novel Bayesian multiscale method for speckle removal in medical ultrasound images," *IEEE Trans. on Medical Imaging*, vol. 20, no. 8, pp. 772-783, Aug 2001.

[4] S.G. Chang, B. Yu, and M. Vetterli, "Spatially adaptive wavelet thresholding with context modeling for image denoising ," *IEEE Trans. Image Proc.*, vol. 9, no. 9, pp. 1522–1531, Sep 2000.

[5] H.A. Chipman, E.D. Kolaczyk, and R.E. McCulloch, "Adaptive Bayesian wavelet shrinkage," *J. of the Amer. Statist. Assoc.*, vol. 92, pp. 1413–1421, 1997.

[6] M.S. Crouse, R.D. Nowak, and R.G. Baranuik, "Wavelet-based statistical signal processing using hidden Markov models," *IEEE Trans. Signal Proc.*, vol. 46, no. 4, pp. 886–902, April 1998.

[7] D.L. Donoho, "De-noising by soft-thresholding," *IEEE, Trans. Inform. Theory*, vol. 41, no. 5, pp. 613–627, May 1995.

[8] W.A. Edelstein, G. Glover, C. Hardy, and R. Redington, "The intrinistic signal-to-noise ratio in NMR imaging," *Magn. Reson. Med*, vol. 3, pp. 604–618, 1986.

[9] Y. Ephraim and D. Malah, "Speech enhancement using a minimum mean-square error short-time spectral amplitude estimation," *IEEE Trans. Acoust. Speech and Signal Proc.*, vol. 32, no. 6, pp. 1109–1121, Dec 1984.

[10] G. Fan and X.-G. Xia, "Image denoising using local contextual hidden Markov model in the wavelet domain," *IEEE Signal Processing Letters*, vol. 8, no. 5, pp. 125–128, May 2001.

[11] S. Foucher, G. B. Benie, and J. M. Boucher, "Unsupervised multiscale speckle filtering," *Proc. IEEE Internat. Conf. on Image Proc ICIP96*, pp. 391–394, Lausanne, Switzerland, 1996.

[12] S. Foucher, G. B. Benie, and J. M. Boucher, "Multiscale MAP filtering of SAR images," *IEEE Trans. Image Proc.*, vol. 10, no. 10, pp. 49–60, January 2001.

[13] J. W. Goodman, "Some fundamental proprerties of speckle," *J. Opt. Soc. Am.*, vol. 66, pp. 1145–1150, 1976.

[14] H. Gudbjartsson and S. Patz,"The Rician distribution of noisy MRI data ," *Magn. Reson. Med*, vol. 34, pp. 910–914, 1995.

[15] T.-C. Hsung, D.P.-K. Lun, and W.-C. Siu, "Denoising by singularity detection," *IEEE Trans. Signal Proc.*, vol. 47, pp. 3139–3144, 1999.

[16] A.K. Jain, *Fundamental of Digital Image Processing*, Prentice-Hall, 1989.

[17] M. Jansen and A. Bultheel, "Geometrical priors for noise-free wavelet coefficient configurations in image de-noising," in *Bayesian inference in wavelet based models*, P. Müller and B. Vidakovic, editors, Springer Verlag 1999, pp. 223–242.

[18] G. Kossof, W.J. Garret, D. A. Carpenter, J. Jellins, and M. J. Dadd, "Principles and classification of soft tissues by gray scale echography," *Ultrasound Med. Biol.*, vol. 2, pp. 89-105, 1976.

[19] H. Krim and I.C. Schick, "Minimax description length for signal denoising and optimized representation," *IEEE Trans. Inform. Theory.*, vol. 45, no. 3, April 1999.

[20] D. Leporini, J.-C. Pasquet and H. Krim, "Best basis representation with prior statistical models," in *Lecture Notes in Statistics*, P. Müller and B. Vidakovic, editors, Springer Verlag 1999, pp. 155–172.

[21] X. Li and M. Orchard, "Spatially adaptive denoising under overcomplete expansion," *Proc. IEEE Internat. Conf. on Image Proc., ICIP00*, Vancouver, Canada, Sep 2000.

[22] A. Macovski, "Noise in MRI," *Magn. Reson. Med*, vol. 36, pp. 494–497, 1996.

[23] M. Malfait and D. Roose, "Wavelet-based image denoising using a Markov random field a priori model," *IEEE Trans. Image Proc.*, vol. 6, no. 4, pp. 549–565, Apr 1997.

[24] S. Mallat, "A theory for multiresolution signal decomposition: the wavelet representation," *IEEE Trans. Pattern Anal. and Machine Intel.*, vol. 11, no. 7, pp. 674-693, July 1989.

[25] S. Mallat, *A wavelet tour of signal processing*, Academic Press, 1998.

[26] R. J. McAulay and M. L. Malpass, "Speech Enhancement Using

a Soft-Decision Noise Suppression Filter," *IEEE Trans. Acoust. Speech and Signal Proc.*, vol. 28, pp. 137–144, Apr 1980.

[27] E.R. McVeigh, R.M. Henkelman, and M.J. Bronskill,"Noise and filtration in magnetic resonance imaging," *Med. Phys.*, vol. 3, pp. 604–618, 1985.

[28] D. Middleton and R. Esposito, "Simultaneous optimum detection and estimation of signals in noise," *IEEE Trans. Inform. Theory*, vol. 14, no. 3, pp. 434–443, May 1968.

[29] M. K. Mihçak, I. Kozintsev, K. Ramchandran, and P. Moulin, "Low-complexity image denoising based on statistical modeling of wavelet coefficients," *IEEE Signal Proc. Letters*, vol. 6, no. 12, pp. 300–303, Dec 1999.

[30] R.D. Nowak, "Wavelet-based Rician noise removal for magnetic resonance imaging," *IEEE Trans. Image Proc.*, vol. 8, pp. 1408–1419, Oct 1999.

[31] A. Pižurica, W. Philips, I. Lemahieu, and M. Acheroy, "A joint inter- and intrascale statistical model for Bayesian wavelet based image denoising," *IEEE Trans. Image Proc.*, vol. 11, no. 5, pp. 545–557, May 2002.

[32] A. Pižurica, "Image denoising using wavelets and spatial context modeling," PhD thesis, Ghent University, Ghent, Belgium, 2002.

[33] A. Pižurica, W. Philips, I. Lemahieu, and M. Acheroy, "Despeckling SAR images using wavelets and a new class of adaptive shrinkage functions," *Proc. IEEE Internat. Conf. on Image Proc., ICIP 2001*, Thessaloniki, Grece, Oct 2001.

[34] F. Sattar, L. Floreby, G. Salomonsson and B. Lövström, "Image enhancement based on a nonlinear multiscale method," *IEEE Trans. Image Proc.*, vol. 6, no. 6, pp. 888–895, June 1997.

[35] F.G. Sommer, L.F. Joynt, B.A. Carroll, and A. Macowski, "Ultrasonic characterization of abdominal tissues via digital analysis of backscattered waveforms," *Radiology*, vol. 141, pp. 811-817, Dec 1981.

[36] M. Unser, and A. Aldroubi, "A review of wavelets in biomedical applications ," *Proc. of the IEEE*, vol. 84, no. 4, pp. 626–634, Apr 1996.

[37] B. Vidakovic, "Wavelet-based nonparametric Bayes methods", in *Practical Nonparametric and Semiparametric Bayesian Statistics*, Lecture Notes in Statistics 133, D.D. Dey, P. Müller and D. Sinha, editors, Springer-Verlag, pp. 133–155, 1998.

[38] Y. Xu, J. B. Weaver, D. M. Healy, J. Lu, "Wavelet transform domain filters: a spatially selective noise filtration technique," *IEEE Trans. Image Proc.*, vol. 3, no. 6, pp. 747–758, Nov. 1994.

[39] R.F. Wagner, S.W. Smith, J.M. Sandrik, and H. Lopez, "Statistics of speckle in ultrasound B-scans," *IEEE Trans. on Sonics and Ultrasonics*, vol. 30, no. 3, pp 156–163, May 1983.

[40] J. Weaver, Y. Xu, D. Healy, and J. Driscoll, "Filtering MR images in the wavelet transform domain," *Magn. Reson. Med*, vol. 21, pp 288-295, 1991.